Computers in Biology and Medicine 110 (2019) 8–14

Contents lists available at ScienceDirect

Computers in Biology and Medicine

journal homepage: www.elsevier.com/locate/compbiomed

Automatic discrimination of neoplastic epithelium and stromal response in breast carcinoma

Massimo Salvi[a,*], Filippo Molinari[a], Natalia Dogliani[b], Martino Bosco[b]

[a] Biolab, Department of Electronics and Telecommunications, Politecnico di Torino, 10129, Turin, Italy
[b] Department of Pathology, Ospedale San Lazzano, 12051, Alba, Italy

ARTICLE INFO

Keywords:
Computer-aided image analysis
Digital pathology
Automatic segmentation
Breast carcinoma
Artificial neural networks

ABSTRACT

Background and objectives: In breast carcinoma, epithelial–stromal interactions play a pivotal role in tumor formation and progression, and it must be accurately assessed for a correct extraction of predictive and prognostic biomarkers. Evaluation of preoperative (baseline) neoplasia/stroma ratio and the enumeration of tumor infiltrating lymphocytes (TIL) represent only two conditions in which precise discrimination of cancer epithelium and stromal reaction are relevant. However, subjectivity and expertise of the operators may lead to different degrees of assessment.

Methods: In this paper, we present a fully automated method for the discrimination between neoplastic epithelium and stromal reaction in breast carcinoma. Starting from cell nuclei, the proposed method implements computer vision strategies to split the neoplastic epithelium tissue from the stromal reaction.

Results: The algorithm is tested on 100 H&E (hematoxylin and eosin) stained images representative of 10 different cases of invasive carcinoma. The algorithm performance in the detection of neoplastic epithelium (compared to manual annotations by an expert pathologist) gave a $F1_{SCORE}$ of 0.8894 and mean $jaccard_{INDEX}$ of 0.8481.

Conclusions: To the best of our knowledge, the proposed method is the first fully automated algorithm for the discrimination between neoplastic epithelium and stromal reaction in H&E stained images of breast tissue. The proposed approach paves the way for an automated and quantitative analysis of predictive and prognostic biomarkers in breast carcinoma.

1. Introduction

The analysis of histological images of breast carcinoma is the standard clinical practice for the diagnosis and prognosis of breast cancer development. In routine histology, the most widely used staining method to visualize tissues is hematoxylin and eosin (H&E), which allow to distinguish cell nuclei (bluish color - hematoxylin) from cytoplasm (pinkish color - eosin) [1]. Pathologists manually perform the tissue analysis under a microscope and their experience directly influence the accuracy of the diagnosis [2].

A generally underrated problem related to image analysis of cancer on histopathological slides is the correct identification of neoplastic epithelium and its distinction from stromal reaction. In most cases, the focus is on the neoplastic epithelium where morphological measures (nuclear pleomorphism, glands formation) and immuno-phenotypical quantifications (proteins expression) are performed. In other cases, the stromal component is analyzed (quantification of tumor infiltrating lymphocytes, characterization of stromal reaction type). In both cases, morphological and immuno-phenotypic characterization of the tumor can predict the breast carcinoma behavior and its prognosis [3–5] and, of course, should only be evaluated on the correct tumor component (epithelial vs stromal). In addition, the direct estimation of tumor/stroma ratio (the ratio of tumor volume occupied by neoplastic epithelium and stroma) has relevance in the determination of the pathological response to neoadjuvant therapy [6] and represents a novel prognostic parameter [7].

Since most of the current pathology diagnosis processes are based on the subjective opinion of pathologists, solutions for the quantitative assessment of histological images would have scope of application. In particular, an automatic system for the analysis of histological breast tissue could assist pathologists by providing objective results, quantitative measurements or even a second opinion.

In the last decade, several algorithms have been proposed for the automatic analysis of breast carcinoma [8–10]. These methods are

* Corresponding author. Biolab, Department of Electronics and Telecommunications, Politecnico di Torino, Corso Duca degli Abruzzi 24, 10129, Torino, Italy.
E-mail address: massimo.salvi@polito.it (M. Salvi).

https://doi.org/10.1016/j.compbiomed.2019.05.009
Received 15 January 2019; Received in revised form 10 May 2019; Accepted 10 May 2019

based on multi-resolution algorithms [11,12], nuclear features [13,14], and deep neural networks [15–17] to perform cancer detection and grading. In particular, deep neural networks have driven advances in image recognition and they achieved state-of-art performance in many segmentation tasks of medical imaging. Above all, convolutional neural networks (CNNs or Mask RCNNs) have shown promising results in the analysis of histological images. Conceptually, these techniques act like classifiers, which are trained to recognize the presence or the absence of tumoral tissue within the [18] image. None of them is specifically designed to discriminate between neoplastic epithelium and stromal response. Furthermore, these methods do not perform a segmentation of the tumor areas; hence, they cannot provide accurate contours of the cancer tissue. This is also due to the extreme inter-tumoral and intra-tumoral variability of neoplastic epithelium morphology, which is a major challenge for an automatic segmentation of the cancer area.

To the best of our knowledge, no fully-automated solutions have been proposed so far for the segmentation of neoplastic epithelium in H &E stained images of breast tissue. In this paper, we present an adaptive and automatic method for the discrimination between neoplastic epithelium and stromal response in breast carcinoma. The proposed algorithm is tested on 100 H&E stained images representative of 10 breast cancer cases and automatic results are compared with manual annotations made by an expert pathologist. In the following section, an exhaustive description of the method is provided.

2. Materials and method

2.1. Image database

Our dataset consists of 100 H&E stained images from 10 different cases of invasive non-special type (according to WHO 2012 classification [19]) carcinoma. Each image is extracted with a fixed dimension of 600x1200 pixel from a whole-slide scan digitalized at 20x magnification. 50 images include both neoplastic epithelium and stromal reaction, 25 has only neoplastic epithelium and 25 images are extracted without cancer tissue in the field-of-view. One expert pathologist (M.B.) manually annotated the neoplastic epithelium contours in each image. The overall dataset composition is shown in Table 1.

2.2. Algorithm architecture

The proposed algorithm is designed to automatically detect neoplastic epithelium contours in H&E stained images of breast tissue. The algorithm is developed using MATLAB (MathWorks, Natick, MA, USA) environment and runs on a workstation with a 3.5 GHz octa-core CPU and 64-GB of RAM. The procedure of the proposed method is schematically described in Fig. 1. Two main steps compose the processing: i) nuclei segmentation and classification, ii) neoplastic epithelium detection. In the following sections, a detailed description of the algorithm is provided.

2.2.1. Nuclei segmentation and classification

The first step of the algorithm is the cell nuclei segmentation inside the image. This task is performed using a multi-tissue and multi-scale approach for nuclei detection adopted in our previous works [20,21]. Briefly, the RGB image of the histological specimen (Fig. 2a) is converted into grayscale and a novel object-based detection is applied to obtain a raw mask of nuclei. Then, area-based corrections and nuclei separation are performed to identify the cells boundaries (Fig. 2b).

Table 1
Dataset composition.

Tissue condition	#Images
Neoplastic epithelium and stromal reaction	50
All neoplastic epithelium	25
No neoplastic epithelium	25
Total	**100**

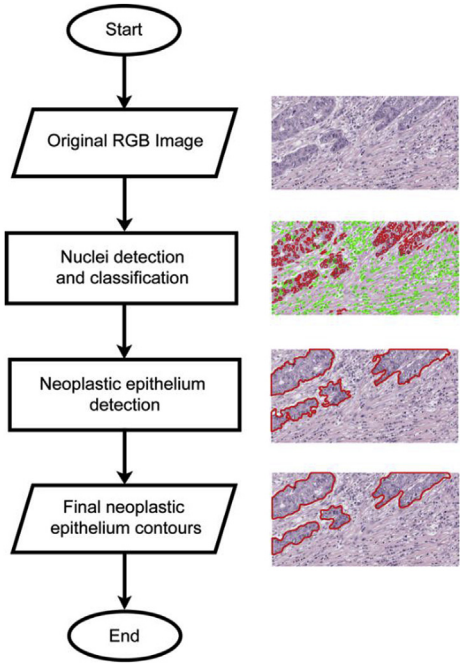

Fig. 1. Schematic representation of the proposed algorithm.

In order to find tumor areas, each nucleus needs to be classified according to a certain pattern (*tumor* or *no-tumor*). A feed-forward artificial neural network (ANN) is used to classify each cell. Five images were randomly selected to train the network. For each image, the pathologist manually drew all nuclei and assigned a pattern for each of them. Then, the total number of nuclei (9316) was randomly divided into 3 sets: the training set (70% = 6522 cells), development set (15% = 1397 cells), and test set (15% = 1397 cells). Five first-order texture descriptors [22,23] were extracted from each cell and used as input features for the ANN: *mean*, *variance*, *skewness*, *kurtosis* and *entropy*. The detailed features description is provided in Table 2. Nuclear texture is used to classify each cell as cancer nuclei have a distinct morphology characterized by coarse chromatin texture [24].Where N indicates the cell area, $I(x,y)$ denotes the grayscale image of the nucleus and p represents its normalized histogram.

In order to understand the feature's relation to the response variable (tumor/no-tumor nuclei), the Pearson correlation coefficient is also computed [25]. All five input features are used to train the neural network because, for each of them, the absolute value of the Pearson coefficient is always higher than 0.3. Feature standardization is applied to obtain variables with zero-mean and unit-variance. During network training, the Levenberg-Marquardt backpropagation [26] and the mean squared normalized error (mse) are used as optimization algorithm and cost function respectively. Finally, the number of epochs is set to 100.

Several network configurations were tested, varying the network parameters (#units, #layers, activation functions and learning rate) and, for each configuration, the errors on the train and dev sets were evaluated. The optimal neural network was chosen in two steps. First of all, the ANNs with a maximum difference between the train and development error equal to 3% were selected to avoid overfitting. Among these, the optimal configuration is chosen as the one with the minimum train/dev mean error to ensure best performance. The optimal network is then used to classify all the cell nuclei detected by the proposed algorithm (Fig. 2c).

Since some nuclei can be misclassified, an iterative three-steps refining process is applied to better define the tumor areas:

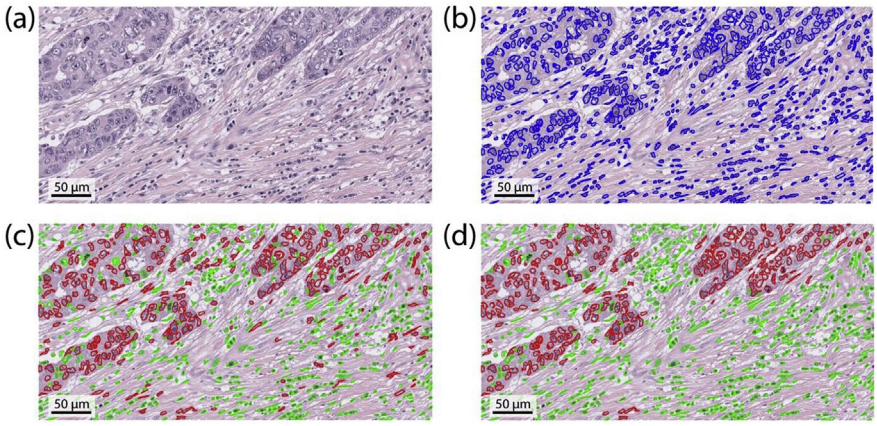

Fig. 2. Nuclei detection and classification. (a) original RGB image, (b) nuclei detection, (c) raw nuclei classification (red: tumor nuclei, green: no-tumor nuclei), (d) nuclei classification after refining process. (For interpretation of the references to color in this figure legend, the reader is referred to the Web version of this article.)

Table 2
Input features of the artificial neural network to perform nuclei classification.

Feature	Mathematical definition
Mean (m)	
Variance (σ^2)	
Skewness (S_k)	
Kurtosis (K_t)	
Entropy (E)	

1. For each cell classified as *no-tumor*, a Region of Interest (ROI) of 40 × 40 μm surrounding that cell is defined. If inside that ROI at least 95% (*conversion percentage*) of the nuclei has been classified as *tumor*, then the cell is now labeled as *tumor*;
2. For each cell classified as *tumor*, a Region of Interest (ROI) of 40 × 40 μm is also defined. If inside that ROI at least 95% of the nuclei has been classified as no-*tumor*, then the cell is now labeled as *no-tumor*;
3. Lowering of the *conversion percentage* by 5%. These steps are repeated until the conversion percentage reaches 75%.

The procedure described above allowed to decrease the number of misclassified nuclei. An example of the refining process is shown in Fig. 2d.

2.2.2. Neoplastic epithelium detection

Once performed nuclei detection and classification, only nuclei labeled as *tumor* are considered for the next steps of the processing (Fig. 3a). Centroids of tumor cells are extracted, and a density-based clustering is performed to segment tumor areas. In particular, a spatial clustering named DBSCAN (Density-Based Spatial Clustering of Application with Noise) is applied to each nuclei centroid [27]. This algorithm finds neighbors of data points, within a circle of radius ε, and adds them into same cluster. For any neighbor point, if its ε-neighborhood contains at least a predefined number of points (min_{POINTS}), the cluster is expanded to contain its neighbors, as well. However, if the number of points in the neighborhood is less than min_{POINTS}, the point is considered to be noise and it is deleted. An iterative two-steps DBSCAN is performed by the proposed method, starting from $\varepsilon = 200$ μm and $min_{POINTS} = 5$. We choose an initial ε-neighborhood of 200 μm as it represents the average cell density in the tumor zones while we set a min_{POINTS} equal to 5 since a tumor area has always more than 5 cells. The iterative DBSCAN follows two steps:

1. Application of the DBSCAN on nuclei centroids using the current values of ε and min_{POINTS};
2. Comparison between the number of cells before and after the clustering. If the difference is less than 5%, ε is decreased by 20 μm and the algorithm returns to step 1.

These two steps are repeated until more than 5% of nuclei are deleted by DBSCAN or ε reaches 50 μm. In this way, the clustering sensitivity is adapted for each image by varying the neighborhood size (ε). The application of the iterative DBSCAN is shown in Fig. 3b. The refining process (section 2.2.1) is essential for the DBSCAN performance. In fact, in the presence of healthy cells inside tumor areas, the spatial clustering could disconnect the tumor areas with a consequent underestimation of the neoplastic epithelium area. On the other hand, if the tumor cells are scattered within the stroma, the DBSCAN could underestimate the number of clusters and consequentially overestimate the tumor areas. Using the iterative process as preprocessing step, it is possible to maximize the performance of the spatial clustering (Fig. 3b). For each cluster, the proposed method extracts the circumscribed polygon to all the nuclei of that cluster (Fig. 3c). However, the result obtained is still sub-optimal, so further steps are performed to get an accurate contour of the neoplastic epithelium.

The proposed method applies an active contour model to improve the detection of tumor borders. In particular, the Chan-Vese region-based energy model is implemented as described in Ref. [28]. This model could detect objects whose boundaries are not necessarily defined by gradient. The Chan-Vese active contours is based on techniques of curve evolution [29], Mumford–Shah functional for segmentation [30] and level sets [31]. For each image of the dataset, this model allows to obtain accurate contours of tumor areas, even if the gradient between neoplastic epithelium and stromal response was very low. The Chan-Vese active contours is applied to the image $I_1 = I_R - I_B$, where I_R and I_B are the red and blue channels of the considered image I, respectively. This channel subtraction aims to brighten the stromal response while simultaneously darkening everything belonging to the neoplastic epithelium (Fig. 3d). The tumor polygons obtained in the previous step are used as the initial contour at which the evolution of the segmentation begins, and the number of iterations is set to 100. The result obtained after the application of Chan-Vese model is illustrated in Fig. 3e.

Morphological operators are then applied to tumor areas to obtain smoother contours. This process is composed of three steps: i) morphological erosion using a disk with 5 μm radius, ii) removal of areas smaller than 100 μm^2 and iii) morphological dilation using the same structural element of the previous erosion. Finally, boundaries between neoplastic epithelial and stromal response are interpolated using the Savitzky-Golay filter [32]. The polynomial order is set to 11 with a window size of 201. The final result provided by the proposed method is shown in Fig. 3f.

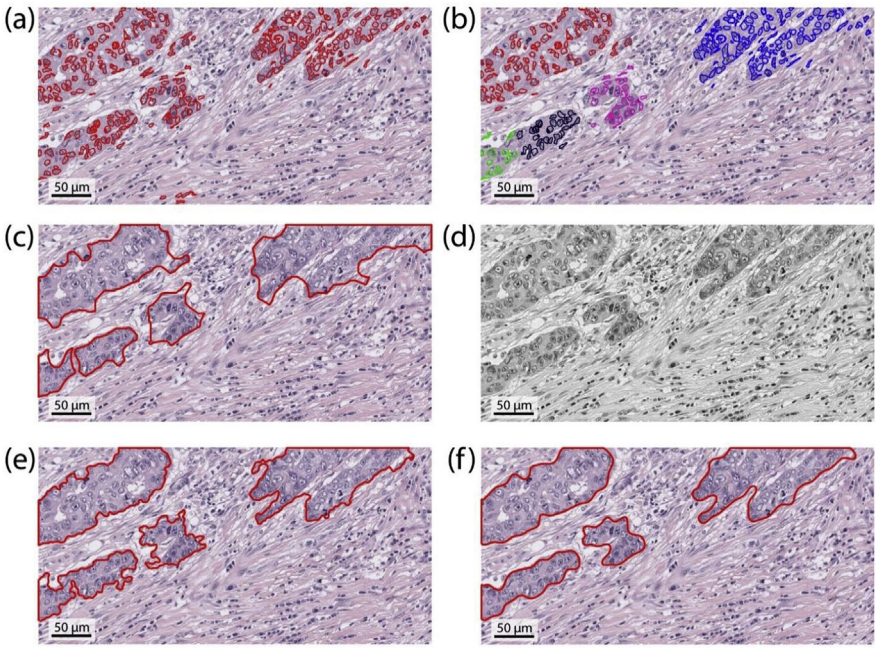

Fig. 3. Neoplastic epithelium detection. (a) nuclei classified as tumor, (b) density-based nuclei clustering (each color represents one cluster), (c) circumscribed polygon for each tumor zone, (d) starting image for active contours (e) tumor boundaries after active contours, (f) final neoplastic epithelium contours. (For interpretation of the references to color in this figure legend, the reader is referred to the Web version of this article.)

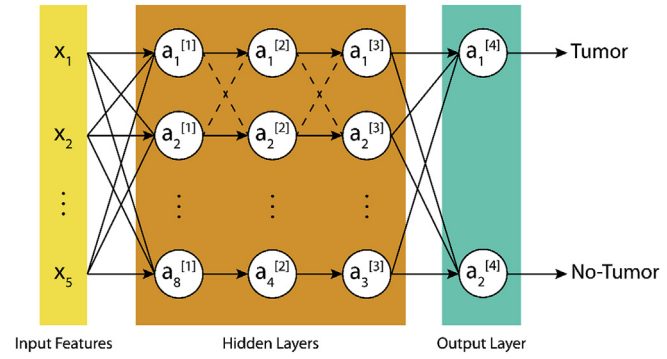

Fig. 4. Neural network architecture for nuclei classification.

Finally, one of the three tissue conditions is associated to each image following these rules:

1. If the whole image is recognized as a tumor area, then the tissue condition is *all neoplastic epithelium*;
2. If there is no tumor area, then the tissue condition is *no neoplastic epithelium*;
3. In all other cases the tissue condition is *neoplastic epithelium and stromal reaction.*

2.3. Performance measures

A comparison between masks drawn by a manual operator ($MASK_{MANUAL}$) and those provided by the proposed method ($MASK_{AUTOMATIC}$) is carried out to assess the algorithm performance in the segmentation of neoplastic epithelium. True positive (TP) is the number of pixels in common between manual and automatic masks, false negative (FN) denotes all pixels not identified by the algorithm and false positive (FP) represents all the pixels identified by the automatic method but not by the manual operator. The segmentation performance is evaluated by calculating the *sensitivity*, *specificity*, *precision*, $F1_{SCORE}$ and $jaccard_{INDEX}$, defined as follows:

$$sensitivity = \frac{TP}{TP + FN}$$

$$specificity = \frac{TN}{TN + FP}$$

$$precision = \frac{TP}{TP + FP}$$

$$F1_{SCORE} = \frac{2TP}{2TP + FP + FN}$$

$$jaccard_{INDEX} = \frac{|MASK_{MANUAL} \cap MASK_{AUTOMATIC}|}{|MASK_{MANUAL} \cup MASK_{AUTOMATIC}|}$$

In detail, *sensitivity* measures the missed detection of ground truth shapes, *specificity* assesses the true negative fraction, *precision* evaluates the false detection of ghost objects, $F1_{SCORE}$ is defined as the harmonic mean of sensitivity and precision [33], and the $jaccard_{INDEX}$ measures similarity between two different shapes, defined as the size of the intersection divided by the size of the union of the segmented object [34].

3. Results

The optimal network configuration used in this work has three hidden layers, with respectively 8, 4 and 3 units (Fig. 4). All layers have a tan-sigmoid transfer function while the output layer has a linear transfer function. The network learning rate is set to 0.01. The network for nuclei classification achieves an average accuracy of 94.64% (training set) and 94.29% (development set). In the test set, the network obtains a mean accuracy of 95.22% (with a precision, recall and $F1_{SCORE}$ of 93.35%, 97.77% and 95.51%, respectively). The five random images selected to train the ANN were excluded from the validation process.

The algorithm obtains a 100% of accuracy in the identification of the tissue condition for all the images. An example of manual and automatic segmentation in the three tissue conditions is shown in Fig. 5.

The performance of the proposed method in the discrimination between neoplastic epithelium and stromal response is also assessed. In order to perform this kind of evaluation, images should contain both neoplastic epithelium and stromal response. For this reason, only images labeled as *neoplastic epithelium and stromal response* are used. The results of the comparison between manual and automatic segmentation are summarized in Table 3.

The algorithm can be considered very performing in the detection of neoplastic epithelium, with very high average values of *sensitivity*,

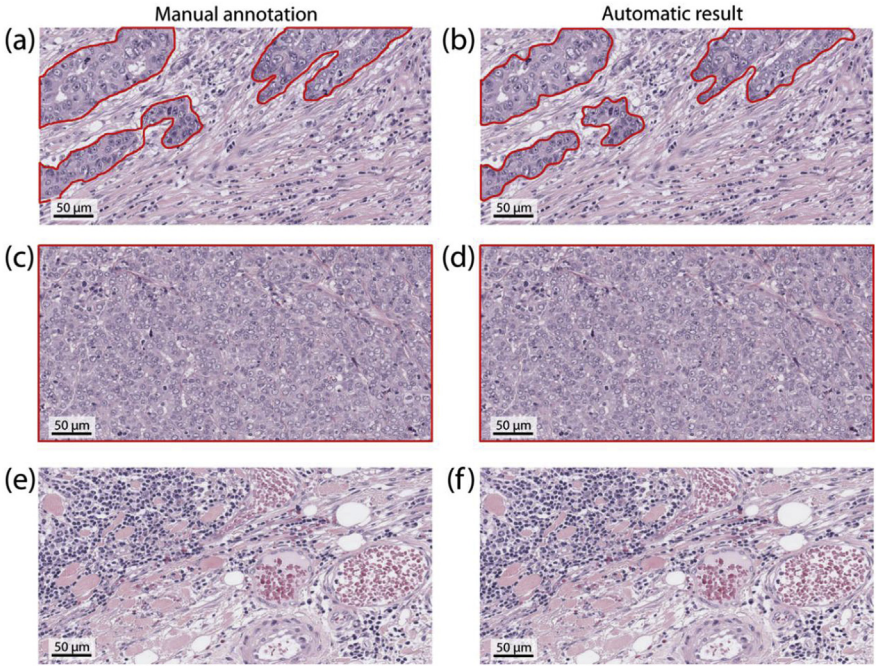

Fig. 5. Comparison between manual and automatic segmentation in the three tissue conditions. First column illustrates the manual annotations while second column shows the corresponding automatic results. (a,b) Image labeled as neoplastic epithelium and stromal response, (c,d) image with all neoplastic epithelium, (e,f) image without neoplastic epithelium.

specificity, *precision*, $F1_{SCORE}$, and $jaccard_{INDEX}$ thus demonstrating the accuracy of the method (Table 3). For all images, *specificity* and *precision* are always higher than 0.90. In addition to being accurate, the proposed method is also fast, with an average computational time of 18.21 s.

Fig. 6 shows some examples of manual and automatic segmentation of neoplastic epithelium in different patients.

4. Discussion

In the present study, we propose a fully automatic method for the discrimination between neoplastic epithelium and stromal reaction in H &E stained images of breast tissue. The distinction between neoplastic epithelium and stromal reaction is essential in the correct extraction of predictive and prognostic biomarkers for breast carcinoma [3,5]. Besides representing an independent prognostic factor, comparison of preoperative (baseline) tumor/stroma ratio on biopsy and after chemotherapy on the surgical specimen is an obligate step for efficacy evaluation of neoadjuvant therapy [6].

Starting from cell nuclei, our technique is able to detect neoplastic epithelium boundaries without any user interaction. The proposed method is tested on 100 H&E stained images of breast tissue and automatic results are compared with manual annotations of an expert pathologist.

The comparison between manual and automatic segmentation shows high performances of the proposed technique (Table 3). In particular, an average $F1_{SCORE}$ of 0.8894 coupled to a mean $jaccard_{INDEX}$ of 0.8481 is obtained. These high performances are mainly due to the combination of an accurate cell nuclei detection/classification and adaptive techniques (spatial clustering and active contours).

The proposed method needs an image acquired with at least 20x magnification otherwise, with a lower resolution, the ANN fails the nuclear texture classification. As a consequence, the algorithm is not able to correctly discriminate between neoplastic epithelium and stromal response. Our method shows excellent performance in images with large extension of tumor areas (Fig. 7a–b). However, the algorithm accuracy slightly decreases with a lobular-structure tumor (Fig. 7c–d) due to the imposed parameters (i.e. settings of the spatial clustering and active contours).

During the algorithm tuning, the two main parameters of DBSCAN (initial value of ε, min_{POINTS}) and the number of iterations of the Chan-Vese active contour model are optimized. Low values of ε (< 200 µm) and min_{POINTS} (< 5) produce an underestimation of tumor areas while too high values of ε (> 200 µm) and min_{POINTS} (> 5) do not allow a correct separation between neoplastic epithelium and stromal response. With a low number of iterations (< 100), the Chan-Vese model fails to adapt itself to the neoplastic epithelium contour so the algorithm does not perform an accurate segmentation of the tumor boundaries. On the other hand, high values of iteration (> 100) causes a rise of the computational time without leading to an increase in performance. The sensitivity analysis of the DBSCAN and Chan-Vese parameters is outlined in Table 4.

The proposed method exhibits excellent performance in images of invasive non-special type carcinoma, but future studies are required to test the accuracy of our algorithm for tumor segmentation in other types of cancer like tubular and lobular breast carcinoma. In the future, automated systems for tumor characterization in whole-slide tissue can be easily developed thanks to the speed and robustness of the proposed method.

5. Conclusion

In this paper, an adaptive algorithm for the automatic discrimination between neoplastic epithelium and stromal response in breast carcinoma is presented. To the best of our knowledge, the proposed method is the first fully automated algorithm for the segmentation of neoplastic epithelium in H&E stained images of breast tissue.

Table 3
Performance of the proposed method in the discrimination between neoplastic epithelium and stromal response. Data are reported as mean ± standard deviation.

Tissue condition	Computational Time (sec)	Sensitivity	Specificity	Precision	F1SCORE	jaccardINDEX
Neoplastic epithelium and stromal reaction	18.11 ± 3.86	0.8680 ± 0.0418	0.9407 ± 0.0683	0.9326 ± 0.0660	0.8894 ± 0.0736	0.8481 ± 0.1114

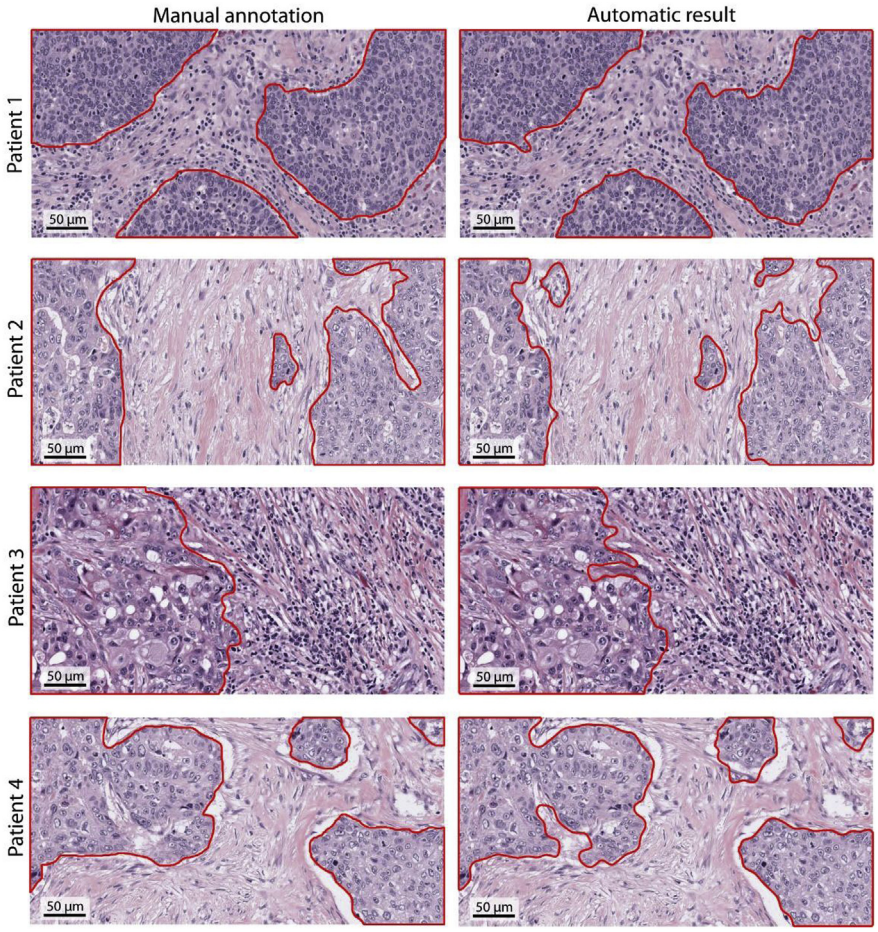

Fig. 6. Comparison between manual and automatic segmentation of the neoplastic epithelium for four different patients, showing challenging cases with high variation of staining intensities, cells morphology and tumor-stromal architecture.

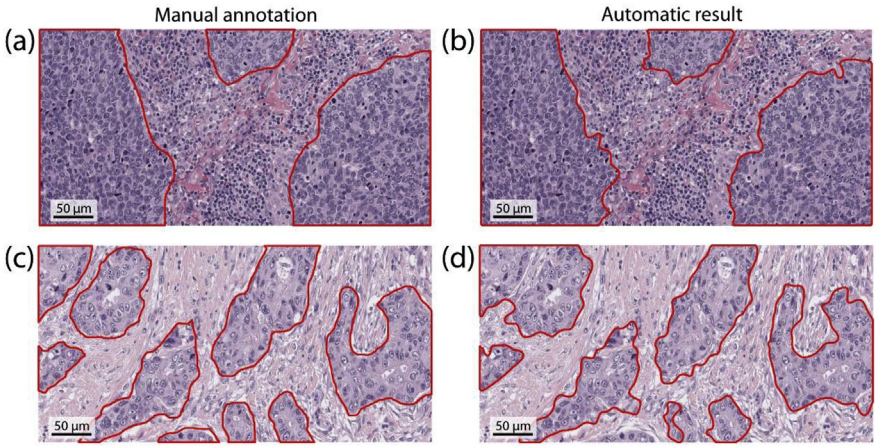

Fig. 7. Comparison between manual and automatic segmentation for two representative samples. First column illustrates the manual annotations while second column shows the corresponding automatic results. (a,b) Image with large extension of tumor areas, (c,d) image with a lobular-structure cancer.

The algorithm is tested on 100 H&E images with high variation of staining intensities (e.g. first vs. Second row of Fig. 6), cells morphology (e.g. Fig. 5c vs Fig. 5e) and tumor-stroma architecture (e.g. third vs. last row of Fig. 6). High segmentation performances are obtained for each image of the dataset.

Being totally automated, this algorithm could be used in future studies as starting point to realize reliable systems for the morphological immunophenotypical tumor characterization and diagnosis. Another possible application of the algorithm is the evaluation of tumor responsiveness to neoadjuvant therapy by means of the determination of the relative fraction of the tumor volume occupied by neoplastic epithelium and stroma before and after the administration of chemotherapy [6]. Our research group is currently working on an extension of this algorithm for the automatic quantification of the biomarkers expressed by stromal cells near the tumor boundary.

Table 4
Sensitivity analysis of the proposed method for the DBSCAN and Chan-Vese parameters. The optimal value for each parameter is highlighted in boldface.

Parameter	Value	Sensitivity	F1SCORE
Initial value of ε (DBSCAN)	50	0.7157 ± 0.0583	0.8203 ± 0.0630
	200	**0.8680 ± 0.0418**	**0.8894 ± 0.0736**
	500	0.8266 ± 0.0427	0.8542 ± 0.0548
min_{POINTS} (DBSCAN)	3	0.7721 ± 0.0393	0.8458 ± 0.0791
	5	**0.8680 ± 0.0418**	**0.8894 ± 0.0736**
	7	0.8384 ± 0.0498	0.8523 ± 0.0654
Number of iteration (Chan-Vese)	50	0.8521 ± 0.0340	0.8604 ± 0.0592
	100	**0.8680 ± 0.0418**	**0.8894 ± 0.0736**
	300	0.8680 ± 0.0418	0.8894 ± 0.0736

Conflicts of interest

The authors have no conflicts of interest.

Acknowledgments

The authors would like to acknowledge all the histology lab technicians of Ospedale San Lazzaro for the technical support.

Appendix A. Supplementary data

Supplementary data to this article can be found online at https://doi.org/10.1016/j.compbiomed.2019.05.009.

References

[1] A. H Fischer, K.A. Jacobson, J. Rose, R. Zeller, Hematoxylin and eosin staining of tissue and cell sections, CSH Protoc, 2008, p. prot4986 2008.
[2] C. Demir, B. Yener, Automated cancer diagnosis based on histopathological images: a systematic survey, Rensselaer Polytech. Institute, Tech. Rep. (2005) 1–16.
[3] E.A. Rakha, M.E. El-Sayed, A.R. Green, A.H.S. Lee, J.F. Robertson, I.O. Ellis, Prognostic markers in triple-negative breast cancer, Cancer 109 (2007) 25–32.
[4] C. Denkert, S. Loibl, A. Noske, M. Roller, B.M. Müller, M. Komor, J. Budczies, S. Darb-Esfahani, R. Kronenwett, C. Hanusch, Tumor-associated lymphocytes as an independent predictor of response to neoadjuvant chemotherapy in breast cancer, J. Clin. Oncol. 28 (2009) 105–113.
[5] S. Adams, R.J. Gray, S. Demaria, L. Goldstein, E.A. Perez, L.N. Shulman, S. Martino, M. Wang, V.E. Jones, T.J. Saphner, Prognostic value of tumor-infiltrating lymphocytes in triple-negative breast cancers from two phase III randomized adjuvant breast cancer trials: ECOG 2197 and ECOG 1199, J. Clin. Oncol. 32 (2014) 2959.
[6] S.E. Pinder, E. Provenzano, H. Earl, I.O. Ellis, Laboratory handling and histology reporting of breast specimens from patients who have received neoadjuvant chemotherapy, Histopathology 50 (2007) 409–417.
[7] J. Wu, C. Liang, M. Chen, W. Su, Association between tumor-stroma ratio and prognosis in solid tumor patients: a systematic review and meta-analysis, Oncotarget 7 (2016) 68954.
[8] M. Veta, J.P.W. Pluim, P.J. Van Diest, M.A. Viergever, Breast cancer histopathology image analysis: a review, IEEE Trans. Biomed. Eng. 61 (2014) 1400–1411.
[9] L. He, L.R. Long, S. Antani, G.R. Thoma, Histology image analysis for carcinoma detection and grading, Comput. Methods Progr. Biomed. 107 (2012) 538–556.
[10] E. Rezk, Z. Awan, F. Islam, A. Jaoua, S. Al Maadeed, N. Zhang, G. Das, N. Rajpoot, Conceptual data sampling for breast cancer histology image classification, Comput. Biol. Med. 89 (2017) 59–67.
[11] J.-R. Dalle, W.K. Leow, D. Racoceanu, A.E. Tutac, T.C. Putti, Automatic breast cancer grading of histopathological images, Eng. Med. Biol. Soc. 2008. EMBS 2008. 30th Annu, . Int. Conf. IEEE, IEEE, 2008, pp. 3052–3055.
[12] D.K. Das, P.K. Dutta, Efficient automated detection of mitotic cells from breast histological images using deep convolution neutral network with wavelet decomposed patches, Comput. Biol. Med. 104 (2019) 29–42.
[13] S. Naik, S. Doyle, S. Agner, A. Madabhushi, M. Feldman, J. Tomaszewski, Automated gland and nuclei segmentation for grading of prostate and breast cancer histopathology, Biomed. Imaging from Nano to Macro, 2008, 5th IEEE Int. Symp., IEEE, 2008, pp. 284–287 ISBI 2008.
[14] A. Phinyomark, S. Jitaree, P. Phukpattaranont, P. Boonyapiphat, Texture analysis of breast cancer cells in microscopic images using critical exponent analysis method, Procedia Eng 32 (2012) 232–238.
[15] N. Wahab, A. Khan, Y.S. Lee, Two-phase deep convolutional neural network for reducing class skewness in histopathological images based breast cancer detection, Comput. Biol. Med. 85 (2017) 86–97.
[16] M. Karabatak, M.C. Ince, An expert system for detection of breast cancer based on association rules and neural network, Expert Syst. Appl. 36 (2009) 3465–3469.
[17] S. Singh, P.R. Gupta, M.K. Sharma, Breast cancer detection and classification of histopathological images, Int. J. Eng. Sci. Technol. 3 (2010) 4228.
[18] M. Kowal, P. Filipczuk, A. Obuchowicz, J. Korbicz, R. Monczak, Computer-aided diagnosis of breast cancer based on fine needle biopsy microscopic images, Comput. Biol. Med. 43 (2013) 1563–1572.
[19] S.R. Lakhani, WHO Classification of Tumours of the Breast, International Agency for Research on Cancer, 2012.
[20] M. Salvi, F. Molinari, Multi-tissue and multi-scale approach for nuclei segmentation in H&E stained images, Biomed. Eng. Online 17 (2018), https://doi.org/10.1186/s12938-018-0518-0.
[21] M. Salvi, U. Morbiducci, F. Amadeo, R. Santoro, F. Angelini, I. Chimenti, D. Massai, E. Messina, A. Giacomello, M. Pesce, Automated segmentation of fluorescence microscopy images for 3D cell detection in human-derived cardiospheres, Sci. Rep. 9 (2019) 6644.
[22] J. Portilla, E.P. Simoncelli, A parametric texture model based on joint statistics of complex wavelet coefficients, Int. J. Comput. Vis. 40 (2000) 49–70, https://doi.org/10.1023/A:1026553619983.
[23] F. Molinari, C. Caresio, U.R. Acharya, M.R.K. Mookiah, M.A. Minetto, Advances in quantitative muscle ultrasonography using texture analysis of ultrasound images, Ultrasound Med. Biol. 41 (2015) 2520–2532.
[24] A. Chekkoury, P. Khurd, J. Ni, C. Bahlmann, A. Kamen, A. Patel, L. Grady, M. Singh, M. Groher, N. Navab, Automated malignancy detection in breast histopathological images, Med. Imaging 2012 Comput. Diagnosis, International Society for Optics and Photonics, 2012, p. 831515.
[25] S. Wright, Correlation and causation, J. Agric. Res. 20 (1921) 557–585.
[26] J.J. Moré, The Levenberg-Marquardt algorithm: implementation and theory, Numer. Anal. Springer, 1978, pp. 105–116.
[27] K.M. Kumar, R.M. Reddy, A fast DBSCAN clustering algorithm by accelerating neighbor searching using Groups method, Pattern Recogn. 58 (2016) 39–48, https://doi.org/10.1016/J.PATCOG.2016.03.008.
[28] T.F. Chan, L.A. Vese, Active contours without edges, IEEE Trans. Image Process. 10 (2001) 266–277, https://doi.org/10.1109/83.902291.
[29] D. Peng, B. Merriman, S. Osher, H. Zhao, M. Kang, Fronts propagating with curvature-dependent speed: algorithms based on Hamilton-Jacobi formulation, J. Comput. Phys. 155 (1999) 410–438.
[30] D. Mumford, J. Shah, Optimal approximations by piecewise smooth functions and associated variational problems, Commun, Pure Appl. Math. 42 (1989) 577–685.
[31] J.A. Sethian, Level Set Methods and Fast Marching Methods: Evolving Interfaces in Computational Geometry, Fluid Mechanics, Computer Vision, and Materials Science, Cambridge university press, 1999.
[32] S.J. Orfanidis, Introduction to Signal Processing, Prentice Hall, Englewood Cliffs, NJ, 1996.
[33] M. Sokolova, G. Lapalme, A systematic analysis of performance measures for classification tasks, Inf. Process. Manag. 45 (2009) 427–437, https://doi.org/10.1016/J.IPM.2009.03.002.
[34] R. Real, J.M. Vargas, The probabilistic basis of jaccard's index of similarity, Syst. Biol. 45 (1996) 380, https://doi.org/10.2307/2413572.